



UNIVERSITY OF LEEDS

This is a repository copy of *Optimal design of GaN-AlGaN Bragg-confined structures for intersubband absorption in the near-infrared spectral range* .

White Rose Research Online URL for this paper:  
<http://eprints.whiterose.ac.uk/711/>

---

**Article:**

Radovanovic, J., Milanovic, V., Ikonc, Z. et al. (3 more authors) (2003) Optimal design of GaN-AlGaN Bragg-confined structures for intersubband absorption in the near-infrared spectral range. *IEEE Journal of Quantum Electronics*, 39 (10). pp. 1297-1304. ISSN 0018-9197

<https://doi.org/10.1109/JQE.2003.817584>

---

**Reuse**

See Attached

**Takedown**

If you consider content in White Rose Research Online to be in breach of UK law, please notify us by emailing [eprints@whiterose.ac.uk](mailto:eprints@whiterose.ac.uk) including the URL of the record and the reason for the withdrawal request.



[eprints@whiterose.ac.uk](mailto:eprints@whiterose.ac.uk)  
<https://eprints.whiterose.ac.uk/>

# Optimal Design of GaN–AlGa<sub>N</sub> Bragg-Confined Structures for Intersubband Absorption in the Near-Infrared Spectral Range

Jelena Radovanović, Vitomir Milanović, Zoran Ikonić, Dragan Indjin, Vladimir Jovanović, and Paul Harrison, *Senior Member, IEEE*

**Abstract**—A method is proposed for the design and optimization of structural parameters of GaN–AlGa<sub>N</sub> Bragg-confined structures with respect to peak intersubband absorption from the ground to the first excited state,  $1 \rightarrow 2$  electronic transition, in the near infrared spectral range. An above-the-barrier bound state was used to extend the range of transition energies above the values available in conventional quantum wells. Intrinsic polarization fields and nonparabolicity effects were taken into account. The selection of optimal parameters, maximizing the absorption at wavelengths of 1.55 and 1.3  $\mu\text{m}$ , was performed by using a simulated annealing algorithm, and optimal structures with infinite superlattices as confinement regions were thus designed. These optimal parameters were then used to set realistic, finite structures with a small number of layers, the performance of which was re-evaluated by solving the Schrödinger–Poisson equation self-consistently for a few different levels and profiles of doping.

**Index Terms**—Bragg-confined structures, GaN quantum wells, intersubband absorption.

## I. INTRODUCTION

A GREAT DEAL of fundamental and applied research has recently been done on wide bandgap group-III nitride semiconductors [1]–[16] because the electronic and optical properties of GaN and related materials make them convenient for a variety of applications such as laser and light emitting diodes in the blue-green and ultraviolet spectral range [1], or high-power and high-frequency electronic devices [2]. The large values of the conduction band discontinuity ( $\Delta E_c \approx 2$  eV for AlN–GaN interface) make nitride-based quantum wells very interesting for achieving intersubband transitions in the near infrared spectral range, which is important for optical communications. In particular, the characteristic wavelengths of 1.55 and 1.3  $\mu\text{m}$  are accessible in nitride quantum structures, and the very short intersubband relaxation times offer a possible route for achieving ultrafast optical switching for terabits per second optical time-division multiplexing [6], [9], [10].

With this class of applications in mind, we consider in this work the design and optimization of GaN–AlGa<sub>N</sub> Bragg con-

finned (BC) structures for the purpose of achieving maximal intersubband absorption between the ground and the first excited state, at a particular wavelength. The electronic structure is calculated within the envelope function model, and including nonparabolicity as derived from the  $8 \times 8 \mathbf{k} \cdot \mathbf{p}$  model [17]. The effects of the internal (built-in) electric field, due to the spontaneous and piezoelectric polarization in (0001)—grown structures, are taken into account. Both the magnitude and direction of this field may change from layer to layer, depending on layer widths and compositions. It may have a significant influence on electronic and optical properties of these structures, e.g. blue-shifting and decreasing the absorption, as compared to the flat band model [9]. In structures relying on Bragg confinement in order to extend the absorption wavelength range, one has to account for the built-in field in the Bragg part of the structure, as well. In order to design and optimize the BC structure parameters which will deliver maximal absorption at a specified wavelength one may choose to employ some conventional optimization procedures, with a suitably defined target function or “goal.” For an idealized structure with infinite superlattices as Bragg reflectors, amenable to quasianalytic considerations, we use the simulated annealing algorithm, which varies the layer widths and compositions in a search for the combination which best meets the preset criteria. The derived set of optimal parameters is then used to set a realistic structure, with just a few layers in Bragg reflectors, and this is then subject to the full self-consistent Schrödinger–Poisson solution for different doping profiles. The self-consistent solution is too demanding computationally to be incorporated in the optimization procedure itself, so the aim of this second phase is to check whether the realistic system remains sufficiently close to the optimal idealized one.

## II. THEORETICAL CONSIDERATIONS

A Bragg-confined structure is, in fact, a perturbed semiconductor superlattice, whose ideal periodicity is disturbed by one or more thin layers embedded in it. Along with the miniband spectrum, characteristic for the superlattice, this structure also has bound states at energies inside the minigaps, their wavefunctions being spatially localized in these embedded layer(s), which will be called the central region. These bound states can even be found high above the barrier top, implying an effectively increased band offset, and enabling bound-bound transitions at higher energies than would be possible in conventional quantum wells. Since we analyze BC structures based on the

Manuscript received November 13, 2002; revised June 24, 2002.

J. Radovanović is with the Institute of Physics, 11080 Belgrade, Yugoslavia.

V. Milanović is with the School of Electrical Engineering, 11120 Belgrade, Yugoslavia.

Z. Ikonić, D. Indjin, V. Jovanović and P. Harrison are with the Institute of Microwaves and Photonics, School of Electronic and Electrical Engineering, University of Leeds, Leeds LS2 9JT, U.K.

Digital Object Identifier 10.1109/JQE.2003.817584

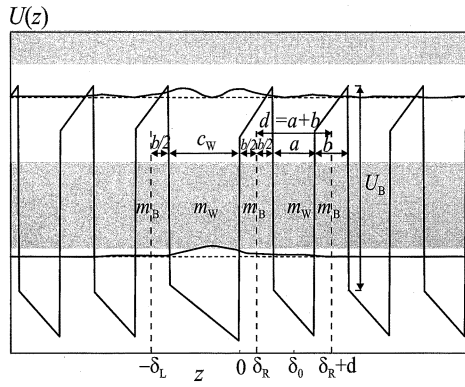


Fig. 1. Band diagram of a GaN–AlGaIn BC structure. Shaded regions denote the superlattice minibands.

$\text{Al}_x\text{Ga}_{1-x}\text{N}$  alloy, it is necessary to include the internal electric field present in every well and barrier region [9], [11]–[13]. Piezoelectric polarization  $P_{PZ}$  is induced by strain due to lattice mismatch between the layers, and can be calculated from [11], [13]:  $P_{PZ} = 2(a_s - a_0)(e_{31} - e_{33}c_{13}/c_{33})/a_0$ , where  $c_{ij}$  and  $e_{ij}$  are the elastic and piezoelectric coefficients, respectively, while  $a_s$  and  $a_0$  denote the lattice constants of the substrate (in our case GaN) and of the structure layers ( $\text{Al}_x\text{Ga}_{1-x}\text{N}$ ). On the other hand, spontaneous polarization is symmetry related and originates from the wurtzite structure of group-III nitrides. It is evaluated as [16]:  $P_{SP}(x) = xP_{\text{AlN}} + (1-x)P_{\text{GaIn}} + bx(1-x)$ , where  $b$  is the bowing parameter. The total polarization  $P$  in a layer is the sum of the two contributions, and the corresponding electric field  $F$  is found by using the interface boundary conditions for polarization, e.g.  $\epsilon_1 F_1 + P_1 = \epsilon_2 F_2 + P_2$ , where  $\epsilon_i$  is the dielectric permittivity of layer  $i$ . The values of  $\epsilon_i$  are not very different for the materials in consideration, and may for simplicity be taken to be the same in all layers, i.e.,  $\epsilon_1 = \epsilon_2 = \epsilon$ . Furthermore, the electric field is calculated using periodic boundary conditions, i.e., taking the total potential drop across the whole structure to be zero. At this point we should note that there is an essential difference between an infinite structure (with two semi-infinite superlattices as Bragg reflectors), and a short finite structure. The infinite structure will clearly have zero potential drop across any single period of the superlattice, because any finite potential difference accumulated in the central, aperiodic part of the structure, will be distributed over infinitely many periods of the superlattice, so to achieve zero global voltage drop. Consequently, all the superlattice periods are here identical, not only structurally but also in terms of the potential, which facilitates analytical considerations. In contrast, in Bragg reflectors with relatively few periods (which may still be quite sufficient for good confinement of wavefunctions) any single period will take a sizeable fraction of the voltage drop in the central part. Therefore, the total potential in a finite structure is not periodic, even though individual periods may be structurally equivalent, which clearly complicates (or simply slows down) considerations of such a system.

The resulting potential profile in a GaN–AlGaIn BC structure is shown in Fig. 1. The superlattice part is a stack of barriers of width  $b$  and wells of width  $a$ , with a potential offset of  $U_B$  at the interface, and this periodicity is perturbed in the center of

the superlattice, in the range  $(-\delta_L, \delta_R)$ , by changing the width of one of the wells.

Bound states in BC structures are usually found within the conventional single-band envelope-function Hamiltonian, which is good enough for states close to the conduction band edge. In nitride-based BC structure however, we are interested in energies high above the conduction band edge, and comparable to the band gap, which requires a more detailed approach, e.g., via the multiband Kane model. In the case of conduction band states, the four-band Kane model may be simplified to an “effectively” two-band model, and further to a single-band model in which the effective mass becomes energy-dependent [18]. The resulting  $2 \times 2$  Hamiltonian, with light-hole (lh) and split-off (so) bands represented by an effective valence band ( $v$ ), reads [18]

$$\hat{\mathcal{H}} = \begin{pmatrix} E_c(z) & \frac{p_{cv}}{m_0} \hat{p}_z \\ -\frac{p_{cv}}{m_0} \hat{p}_z & E_v(z) \end{pmatrix} \quad (1)$$

In this expression,  $E_v = (2E_{\text{lh}} + E_{\text{so}})/3$ , and  $\hat{p}_z = -i\hbar(\partial/\partial z)$ ,  $p_{cv}$  is the momentum matrix element between bulk Bloch states, which can be written as  $p_{cv} = i\sqrt{m_0 E_p}/2$  ( $m_0$  is the free electron mass) and  $E_p$  is the Kane energy ( $\sim 14$  eV in GaN [17]). From (1), one obtains the following differential equation [18]:

$$\hat{p}_z \frac{1}{2m(z, E)} \hat{p}_z \phi_c + E_c \phi_c = E \phi_c \quad (2)$$

where  $\phi_c$  represents the conduction band component of the envelope wave function vector, and the energy-dependent effective mass is given by

$$m(z, E) = m_0 \frac{E - E_v}{E_p} \quad (3)$$

The envelope wavefunctions  $\Psi(z) \equiv \phi_c$  are found here by solving the Schrödinger equation of the form (2), i.e., more precisely

$$-\frac{\hbar^2}{2} \frac{d}{dz} \left( \frac{1}{m(z, E)} \frac{d\Psi}{dz} \right) + U(z)\Psi = E\Psi \quad (4)$$

where the position—and energy—dependent effective mass is calculated as:  $m(z, E) = m(z)[1 + (E - U(z))/E_g(z)]$ , with  $m(z)$ ,  $E_g(z)$ , and  $U(z)$  denoting the parabolic effective mass, band gap, and conduction band edge, respectively. This model predicts rather accurately the bound-state energies, even well above the barrier top. Within this model, the standard expression for the dipole matrix element between states  $i$  and  $j$  of the conduction band  $M_{ij} = \langle \Psi_i | z | \Psi_j \rangle$  becomes incorrect, because the wave functions computed from (4) are not orthogonal (due to the energy dependence of the mass). Therefore, it is necessary to include the valence band contribution into the matrix element, which then reads [18]

$$M_{ij} = \frac{\hbar}{2(E_j - E_i)} \left\langle \Psi_i \left| \hat{p}_z \frac{1}{m(z, E_i)} + \frac{1}{m(z, E_j)} \hat{p}_z \right| \Psi_j \right\rangle. \quad (5)$$

Furthermore, the wavefunctions  $\Psi_i$  and  $\Psi_j$  must be normalized according to [18]

$$\left\langle \Psi_i \left| 1 + \frac{E - U(z)}{E - U(z) + E_g(z)} \right| \Psi_i \right\rangle = 1. \quad (6)$$

Within the asymmetric central layer of the structure shown in Fig. 1, the solution of (4) may be written as

$$\Psi(z) = A_1 y_1(z) + A_2 y_2(z), \quad -\delta_L < z < \delta_R \quad (7)$$

where the functions  $y_1(z)$  and  $y_2(z)$  satisfy the following boundary conditions at  $z = 0$ :  $y_1(0) = 1$ ,  $y_1'(0) = 0$ ,  $y_2(0) = 0$ , and  $y_2'(0) = 1$ . To the left and to the right of this central region, the envelope functions are taken as a linear combination

$$\Psi(z) = C_1 u_{k_z} e^{ik_z z} + C_2 u_{-k_z} e^{-ik_z z}, \quad z < -\delta_L \wedge z > \delta_R \quad (8)$$

where  $k_z$  is the  $z$ -component of the wavevector and  $u_{\pm k_z}(z)$  are the periodic parts of the superlattice envelope Bloch functions, which may be found by considering a single period, of width  $d = a + b$ . These are also taken as a linear combination of particular solutions

$$u_{\pm k_z} e^{\pm ik_z z} = \text{Const} \cdot [y_e(z) + \theta(\pm k_z) y_o(z)] \quad (9)$$

where  $y_e(z)$  and  $y_o(z)$  are the solutions of (4) in the period under consideration,  $\delta_0 - d/2 \leq z < \delta_0 + d/2$ , which satisfy the fundamental boundary conditions at  $z = \delta_0$ . For any other period, these two are found by simple translation. The constant  $\theta$  follows by applying Bloch conditions  $u_{\pm k_z}(\delta_0 - d/2) = u_{\pm k_z}(\delta_0 + d/2)$ , and amounts to

$$\theta = i \frac{y_e \sin\left(\frac{k_z d}{2}\right) - i \left(\frac{\Delta y_e}{2}\right) \exp\left(\frac{ik_z d}{2}\right)}{y_o \cos\left(\frac{k_z d}{2}\right) - \left(\frac{\Delta y_o}{2}\right) \exp\left(\frac{ik_z d}{2}\right)} \quad (10)$$

where the notation  $y_{e,o} \equiv y_{e,o}(\delta_0 + d/2)$ ,  $\Delta y_e \equiv y_e(\delta_0 - d/2) - y_e$ , and  $\Delta y_o \equiv y_o(\delta_0 - d/2) + y_o$  is introduced, and where the product  $k_z d$  is found from the dispersion relation

$$\begin{aligned} \cos(k_z d) &= -\frac{1}{2} \frac{m(\delta_0)}{m(\delta_0 + \frac{d}{2})} (y_o \tilde{y}'_e + y'_e \tilde{y}_o - y_e \tilde{y}'_o - \tilde{y}_e y'_o) \\ &\equiv F(E) \end{aligned} \quad (11)$$

where  $\tilde{y}_{e,o} \equiv y_{e,o}(\delta_0 - d/2)$  and  $\tilde{y}'_{e,o} \equiv y'_{e,o}(\delta_0 - d/2)$ , while  $m(\delta_0)$  and  $m(\delta_0 + d/2)$  denote the electron effective masses in the well and barrier (Fig. 1), with the nonparabolicity effects included. Bound states in the minigaps of this structure correspond to complex values of the wavevector  $k_z$ , which may be written as

$$k_z = \frac{n\pi}{d} + ik_I, \quad (k_I > 0, n = 0, 1, 2, \dots) \quad (12)$$

where  $n$  is the minigap index. From the dispersion relation (11), one then finds

$$k_I d = \text{arccosh}(|F(E)|) \quad (13)$$

because even  $n$  corresponds to  $F(E) > 1$  and odd to  $F(E) < -1$ . If the wavefunction defined by (8) is to remain finite in the limit  $z \rightarrow \pm\infty$ , the constant  $C_1$  has to be zero for  $z < -\delta_L$ , and similarly  $C_2 = 0$  for  $z > \delta_R$ . The bound-state wavefunctions in  $l$ th period of the superlattice, i.e.,  $(-\delta_L - ld < z < -\delta_L - (l-1)d)$  and  $(\delta_R + (l-1)d < z < \delta_R + ld)$ , then reduce to

$$\Psi(z) = B_{L,R} (-1)^{n(l-1)} e^{-(l-1)k_I d} [y_e(z) + \theta_{L,R} y_o(z)] \quad (14)$$

where the subscripts  $L(R)$  denote the region to the left (right) of the central layer. The constant  $\theta$ , from (10) and (12), reads

$$\begin{aligned} \theta_R &= -\frac{y_e \sinh\left(\frac{k_I d}{2}\right) - \left(\frac{\Delta y_e}{2}\right) e^{-\frac{k_I d}{2}}}{y_o \cosh\left(\frac{k_I d}{2}\right) - \left(\frac{\Delta y_o}{2}\right) e^{-\frac{k_I d}{2}}}, \quad n = 0, 2, 4, \dots \\ \theta_R &= -\frac{y_e \cosh\left(\frac{k_I d}{2}\right) + \left(\frac{\Delta y_e}{2}\right) e^{-\frac{k_I d}{2}}}{y_o \sinh\left(\frac{k_I d}{2}\right) + \left(\frac{\Delta y_o}{2}\right) e^{-\frac{k_I d}{2}}}, \quad n = 1, 3, 5, \dots \\ \theta_L &= \theta_R(-k_I) \end{aligned} \quad (15)$$

The continuity of  $\Psi(z)$  and  $[1/m(z)](d\Psi/dz)$  at  $z = -\delta_L$  and at  $z = \delta_R$  then, according to (7) and (14), delivers the linear homogeneous system in constants  $A_{1,2}$  and  $B_{L,R}$ . Equating its determinant to zero results in transcendental equation which should be solved for bound-state energies [19], [20]

$$\begin{aligned} \eta_L \{-\eta_R (\tilde{y}'_1 y'_2 - y'_1 \tilde{y}'_2) + \eta'_R (\tilde{y}'_1 y_2 - y_1 \tilde{y}'_2)\} \\ - \eta'_L \{-\eta_R (\tilde{y}_1 y'_2 - y'_1 \tilde{y}_2) + \eta_R (\tilde{y}_1 y_2 - y_1 \tilde{y}_2)\} = 0 \end{aligned} \quad (16)$$

where  $\eta_L \equiv \tilde{y}_e + \theta_L \tilde{y}_o$ ,  $\eta_R \equiv y_e + \theta_R y_o$ ,  $\tilde{y}_{1,2} \equiv y_{1,2}(-\delta_L)$ , and  $y_{1,2} \equiv y_{1,2}(\delta_R)$ . Having found the solutions of the above equation, the coefficients  $A_{1,2}$ , and  $B_{L,R}$  are found from the normalization condition of bound-state wavefunctions (6).

The quantity of interest in this work is the fractional absorption on the transition  $i \rightarrow f$  between two bound states, which is calculated from

$$A_{if} = \frac{e^2}{2\bar{n}\epsilon_0\omega m_0^2 c} \times \int_0^{+\infty} |P_{if}|^2 F_{if}(k_t^2) \delta(E_f - E_i - \hbar\omega) d(k_t^2) \quad (17)$$

where  $\bar{n}$  is the refractive index,  $c$  the velocity of light,  $\epsilon_0$  is the vacuum dielectric permittivity,  $\hbar\omega$  is photon energy,  $k_t$  is the in-plane wavevector, and  $F_{if}$  denotes the difference of Fermi-Dirac functions for states  $i$  and  $f$ .  $P_{if}$  is the momentum matrix element which may be written as  $P_{if} = -im_0\omega M_{if}$ . In reality, the absorption profile given by (17) is smeared by Lorentz broadening, and the fractional absorption may then be written as

$$A_{if} = \frac{e^2\omega}{2\bar{n}\epsilon_0 c} |M_{if}|^2 \int_0^{+\infty} L(k_t^2) F_{if}(k_t^2) d(k_t^2) \quad (18)$$

where the dipole transition matrix element is taken to be independent of  $k_t$ , and  $L$  is the normalized Lorentzian given by

$$L = \frac{\frac{\Gamma}{2\pi}}{\left[ \hbar\omega - \left( \Delta E_{fi}(0) + \frac{\hbar^2 k_t^2}{2m_{\parallel fi}} \right) \right]^2 + \left[ \frac{\Gamma}{2} \right]^2} \quad (19)$$

where  $\Delta E_{fi}(0)$  is the transition energy at  $k_t = 0$ ,  $\Gamma$  is the homogeneous part of the transition linewidth, and  $m_{\parallel fi}^{-1} = m_{\parallel f}^{-1} - m_{\parallel i}^{-1}$  is the difference of reciprocal in-plane (transversal) electron effective masses in the initial and final state.

At this point, we note that the energy-dependent effective mass (Kane's) model of nonparabolicity, used in calculating the envelope wavefunctions, does not distinguish between the perpendicular (along the quantization axis) and the transverse effects of nonparabolicity. In order to consider this, we followed the alternative approach [21], which uses the nonparabolicity parameters  $\alpha$  and  $\beta$ . To determine these parameters for GaN and AlN, we started with the  $8 \times 8 \mathbf{k} \cdot \mathbf{p}$  Hamiltonian for wurtzite semiconductors [17], diagonalized it at a number of  $\{k_x, k_y, k_z\}$  points, and fitted the results to an expression analogous to that given by Ekenberg [21], but which accounts for the anisotropy that exists in wurtzite materials

$$E(\mathbf{k}) = \frac{\hbar^2}{2m_z} k_z^2 + \frac{\hbar^2}{2m_t} (k_x^2 + k_y^2) + \alpha (k_x^2 + k_y^2 + k_z^2)^2 + \beta_z k_z^2 (k_x^2 + k_y^2) + \beta_t k_x^2 k_y^2. \quad (20)$$

Assuming that  $m_z \approx m_t$  in AlGaIn, as is frequently done, (20) may be written in the form (after collecting the terms with different powers of  $k_z$  separately)

$$E(\mathbf{k}) = \alpha k_z^4 + \left[ \frac{\hbar^2}{2m_z} + (2\alpha + \beta_z) (k_x^2 + k_y^2) \right] k_z^2 + \frac{\hbar^2}{2m_z} (k_x^2 + k_y^2) + (2\alpha + \beta_t) k_x^2 k_y^2 + \alpha (k_x^4 + k_y^4). \quad (21)$$

Following the Ekenberg procedure [21], the transverse effective mass of a quantized state is found as

$$m_{\parallel}(E) \approx m_z [1 + (2\alpha' + \beta'_z)(E - U)] \quad (22)$$

where  $\alpha' = -(2m_z/\hbar^2)^2 \alpha$  and  $\beta'_z = -(2m_z/\hbar^2)^2 \beta_z$ . It is clear from (20) that the analysis of BC structures would be quite involved if using the Ekenberg approach, so the simpler, energy-dependent effective mass formulation was used instead. However, only the former is able to distinguish between the in-plane and perpendicular effects of nonparabolicity, and was used when this difference is important.

Numerical calculation of the nonparabolicity parameters gives [14]:  $\alpha'_{\text{GaN}} = 0.305 \text{ eV}^{-1}$ ,  $\beta'_{z\text{GaN}} = 0.049 \text{ eV}^{-1}$ ,  $\alpha'_{\text{AlN}} = 0.14 \text{ eV}^{-1}$ , and  $\beta'_{z\text{AlN}} = -0.051 \text{ eV}^{-1}$ . With these values, to a very good approximation, we have

$$m_{\parallel}(E) \approx m_z [1 + 2\alpha'(E - U)] \quad (23)$$

and

$$m_{\perp}(E) \approx m_z [1 + \alpha'(E - U)] \quad (24)$$

which implies that the in-plane mass is enhanced over the band edge mass about twice as much as the perpendicular mass. As noted previously [21], though derived for a quantum well in infinitely high barriers, (24) also holds approximately for wells with finite barriers, and the values  $m_z \approx m_{\text{GaN}}$  and  $\alpha' = \alpha'_{\text{GaN}}$

should be used in (24). The rigorous treatment for the case of finite barriers [21] is too involved and is not used in this work.

To find the self-consistent solution all the above expressions are to be used in an iterative procedure of finding the eigenstates of the Schrödinger equation, using those in the Poisson equation

$$\frac{d^2 V}{dz^2} = -\frac{\rho}{\epsilon} \quad (25)$$

to get the electrostatic potential, adding to it the exchange-correlation potential, inserting those back into the Schrödinger equation, etc., until the self consistency is reached. To evaluate  $\rho$  in (25), one has to find the Fermi level  $E_F$  from the global neutrality condition. Here comes another essential difference between an idealized infinite structure and the one with short Bragg reflectors. Infinite structure has allowed minibands, characterized by a finite density of states, and therefore has an infinite total number of states (simply because of its infinite extent). This in turn implies that the presence of a very limited number of bound states, confined to the central part, will have no influence on  $E_F$ . Consequently, the global neutrality condition may be imposed on any single period of the superlattice, in the form:  $\sum_i N_i = N_V$ , where  $N_V$  is the doping per unit well surface per period (i.e. the average volume doping) and  $N_i$  is the electron density in the  $i$ th miniband, which reads

$$N_i = \frac{k_B T}{\pi^2 \hbar^2 d} \times \int_{E_{\min}}^{E_{\max}} \ln \left[ 1 + e^{\frac{E_F - E(k_z, k_t=0)}{k_B T}} \right] \frac{m_{\parallel}(E) F'(E)}{(-1)^i \sqrt{1 - F^2}} dE \quad (26)$$

where  $k_B$  is the Boltzmann constant,  $T$  the temperature, and  $E_{\max, \min}$  are the boundaries of the miniband under consideration. In contrast, a finite structure with short Bragg reflectors has only discrete states: those confined to the central layer, and those to the Bragg reflectors (the latter would merge into minibands only in the limit of very wide Bragg reflectors). In this case, the total electron sheet density is obtained by summing over all discrete states  $i$

$$N_s = \frac{k_B T}{\pi \hbar^2} \sum_i m_{\parallel i} \ln \left[ 1 + \exp \left( \frac{E_F - E_i(k_t=0)}{k_B T} \right) \right] \quad (27)$$

where  $m_{\parallel i}$  is the in-plane effective mass of state  $i$ , and this  $N_s$  is equated to the total sheet doping density  $N_S$  (across the structure).

### III. NUMERICAL RESULTS

We first consider the idealized (infinite) BC structure. It is clear from Fig. 1 that the bound state and miniband positions, and hence the fractional absorption  $A_{12} \sim M_{12}^2$  for the selected transition ( $1 \rightarrow 2$ ), depend on four structural parameters: the layer widths within the superlattice unit cell ( $a$  and  $b$ ), the Al mole fraction  $x$  (which determines the barrier height  $U_B$ ) and the central well width  $c_W$ . The optimization procedure relies on varying their values within physically or technologically feasible limits in order to find the structure with maximal  $M_{12}^2$ , while keeping the transition energy to the required value ( $\Delta E_{21} \approx \hbar\omega$ ). The most convenient and reliable way of performing this task is to use one of the well established methods

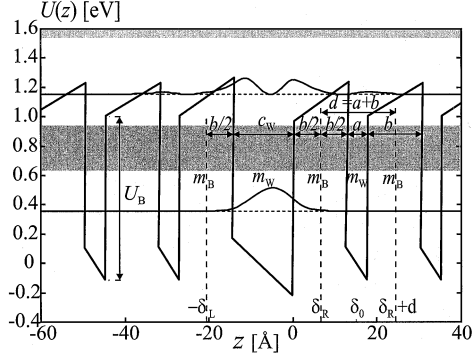


Fig. 2. Band diagram of the central segment of idealized infinite BC structure optimized for intersubband absorption at  $\lambda \sim 1.55 \mu\text{m}$ .

of global optimization, such as simulated annealing [22]. This algorithm enables one to find the optimum of a target function within the specified range of a free parameter space, and has shown good results in optimization of intersubband devices [23]. For the problem considered here, the target function is chosen as

$$J = \frac{M_{12}^2(\Delta E_{21})}{(\Delta E_{21} - \hbar\omega)^2 + \gamma^2}. \quad (28)$$

The role of the denominator is to favor structures which meet the resonance condition ( $\Delta E_{21} \approx \hbar\omega$ ), where  $\gamma$  is a constant guarding against the singular behavior of the target function close to resonance. It should also be noted that all the electrons are assumed to populate the lowest state, and then the precise value of  $E_F$  does not influence the behavior of (28). This assumption has to be checked afterwards.

The material parameters used in the numerical calculations were [24]:  $m_{\text{AlN}} = 0.27m_0$  ( $m_0$  is the free electron mass),  $m_{\text{GaN}} = 0.18m_0$ ,  $E_{g\text{AlN}} = 6.28 \text{ eV}$ ,  $E_{g\text{GaN}} = 3.45 \text{ eV}$ ,  $\bar{n} = 2.74$ ,  $a_s = 3.189 \text{ \AA}$ ,  $a_0 = (3.189 - 0.077x) \text{ \AA}$ ,  $e_{33} = (0.73x + 0.73) \text{ C/m}^2$ ,  $e_{31} = (-0.11x - 0.49) \text{ C/m}^2$ ,  $c_{13} = (103 + 5x) \text{ GPa}$ ,  $c_{33} = (405 - 32x) \text{ GPa}$ ,  $\epsilon \approx 9.5\epsilon_0$ , and  $P_{\text{SP}} = (-0.090x - 0.034(1 - x) + 0.019x(1 - x)) \text{ C/m}^2$ , [16]. The AlN/GaN conduction band offset was taken to be  $\Delta E_c = 2 \text{ eV}$ , as obtained from photoemission spectroscopy measurements [25] and calculations [26]. Vegard's law (linear interpolation) was used for the alloy layers, which is valid in this system [27].

The procedure described above was first performed for a photon energy  $\hbar\omega = 800 \text{ meV}$  ( $\lambda \approx 1.55 \mu\text{m}$ ). The optimal idealized structure deduced in this case had the following parameters:  $a = 5 \text{ \AA}$ ,  $b = 12.6 \text{ \AA}$ ,  $c_w = 14.6 \text{ \AA}$  and  $U_B = 1.123 \text{ eV}$ , as shown in Fig. 2. The relevant bound states are at  $E_1 = 0.355 \text{ eV}$  and  $E_2 = 1.153 \text{ eV}$ , while the miniband boundaries were found from (11). In the structure given in Fig. 2 the first two minibands (which exist in infinite structure) cover the range  $(0.634\text{--}0.941) \text{ eV}$  and  $(1.542\text{--}2.445) \text{ eV}$ . The dependence of the transition dipole matrix elements on some of structural parameters, obtained in course of the optimization procedure, is given in Fig. 3 for a few cases (those providing large values of  $M_{12}$ ). Generally, we find that large values of  $M_{12}$  occur in structures where both discrete states reside near the middle of the minigaps. This is consistent with Bragg

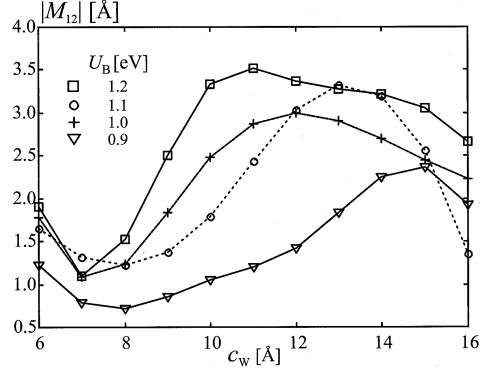


Fig. 3. Dependence of the dipole matrix element on the central well width, plotted for a few different values of the AlGaIn barrier height ( $\Delta E_{21} = 800 \text{ meV}$  in all cases).

reflection conditions, interpreted in terms of layer-averaged wavevectors

$$\begin{aligned} \bar{k}_b b &= \left(r + \frac{1}{2}\right) \pi \\ \bar{k}_a a &= \left(s + \frac{1}{2}\right) \pi, \quad s, r = 0, 1, 2, \dots \end{aligned} \quad (29)$$

where  $\bar{k}_w = (1/w) \int_{(w)} \sqrt{2m(z, E)} |U(z) - E| / \hbar^2 dz$ ,  $w = a, b$ .

It is interesting to note a nonsmooth variation of parameters in Fig. 3 as  $c_w$  varies. This is caused by the fact that any change in  $c_w$  requires redetermination of  $a$  and  $b$  in order to bring the localized state 2 back to the middle of mini-band-gap, keep the transition energy constant, and retain a large matrix element, which sometimes results in substantial changes of  $a$ ,  $b$ , and  $U_B$  (i.e. in an essentially new structure). Taking an example from Fig. 3, for  $c_w = 9 \text{ \AA}$ ,  $a = 17.5 \text{ \AA}$ ,  $b = 16 \text{ \AA}$ , and  $U_B = 1.2 \text{ eV}$  the miniband energies are  $(0.244\text{--}0.264) \text{ eV}$ ,  $(0.866\text{--}0.972) \text{ eV}$ , and  $(1.400\text{--}1.746) \text{ eV}$ , and localized state energies are  $E_1 = 0.585 \text{ eV}$  and  $E_2 = 1.393 \text{ eV}$ , which give the transition matrix element of  $M_{12} = 2.5 \text{ \AA}$ . Almost the same value of  $M_{12} (\approx 2.4) \text{ \AA}$ , and the same transition energy is also obtained with a considerably wider well,  $c_w = 15 \text{ \AA}$ , and other parameters are then  $a = 6 \text{ \AA}$ ,  $b = 9.5 \text{ \AA}$ , and  $U_B = 0.9 \text{ eV}$ ; minibands are then positioned at  $(0.492\text{--}0.984) \text{ eV}$  and  $(1.462\text{--}2.665) \text{ eV}$ , and localized states at  $E_1 = 0.299 \text{ eV}$  and  $E_2 = 1.097 \text{ eV}$ .

The optimization procedure was also performed for another wavelength of interest ( $\lambda \approx 1.3 \mu\text{m}$ , i.e.,  $\Delta E_{21} = 950 \text{ meV}$ ). In this case, the optimal structural parameters were:  $a = 5.1 \text{ \AA}$ ,  $b = 12.9 \text{ \AA}$ ,  $c_w = 10.5 \text{ \AA}$ , and  $U_B = 1.3 \text{ eV}$ . The two relevant bound states are now at  $E_1 = 0.542 \text{ eV}$  and  $E_2 = 1.492 \text{ eV}$ , and the two lowest minibands are at  $(0.728\text{--}0.955) \text{ eV}$  and  $(1.653\text{--}2.416) \text{ eV}$ , as shown in Fig. 4. The dependence of dipole matrix element on some parameters is shown in Fig. 5. Similarly to the previous case, changes of  $c_w$  may result in substantial changes of other parameters. Structures with similar values of  $M_{12} = 1.9 \text{ \AA}$  (for  $c_w = 7 \text{ \AA}$ ) and  $M_{12} = 1.8 \text{ \AA}$  (for  $c_w = 15 \text{ \AA}$ ) have quite dissimilar values of all the other parameters and the corresponding band structures:  $a = 14 \text{ \AA}$ ,  $b = 13 \text{ \AA}$ ,  $U_B = 1.3 \text{ eV}$ , minibands at  $(0.362\text{--}0.402) \text{ eV}$ ,  $(1.148\text{--}1.346) \text{ eV}$ , and  $(1.769\text{--}2.283) \text{ eV}$ , localized states at  $E_1 = 0.780 \text{ eV}$

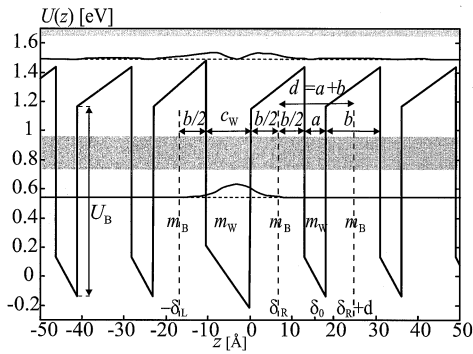


Fig. 4. Same as Fig. 2 but for  $\lambda \sim 1.3 \mu\text{m}$ .

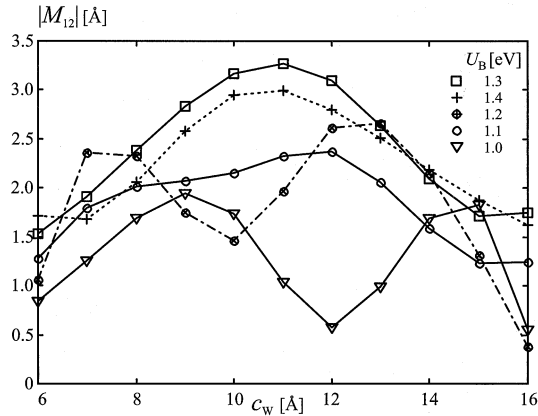


Fig. 5. Same as Fig. 3 but for structures with  $\Delta E_{21} = 950 \text{ meV}$ .

and  $E_2 = 1.730 \text{ eV}$  in the former case, and in the latter case  $a = 6 \text{ \AA}$ ,  $b = 7 \text{ \AA}$ ,  $U_B = 1 \text{ eV}$ , minibands at  $(0.465\text{--}1.261) \text{ eV}$  and  $(1.770\text{--}2.788) \text{ eV}$ , bound states at  $E_1 = 0.322 \text{ eV}$  and  $E_2 = 1.272 \text{ eV}$ . It is worth noting that a conventional quantum well with barrier-confined states, optimized at this short wavelength, would be on the verge of realizability, having a very high Al content in the barrier ( $x \geq 0.9$ ) and a rather narrow well layer [14]. On the other hand, the BC structure shown in Fig. 4, which supports the above-the-barrier confinement, requires a smaller Al content in the barriers ( $x \approx 0.65$ ), which are thus less strained, with less-pronounced critical thickness issues.

Next, we consider realistic Bragg structures, which normally comprise a relatively small number ( $< 10$ ) of superlattice periods for confinement. The structural parameters are taken as found for optimal idealized structures, but at this point we include the effects of doping, i.e., self-consistency. Two types of doping profiles are usually employed [5], either that of the central well only, or that of the two periods of the superlattice on either side of the central well (modulation doping). The sheet electron densities were taken as either  $2 \times 10^{12} \text{ cm}^{-2}$  or  $1 \times 10^{13} \text{ cm}^{-2}$ . The number of superlattice periods was chosen so to provide good confinement of localized states and preserve the designed energy spacing. Larger energies generally demand a larger number of periods. The  $\lambda \approx 1.55 \mu\text{m}$  structure, Fig. 2, really needs just four periods on each side to achieve good confinement. As an example, the self-consistently calculated potential profile in such a structure, with the modulation doping of  $1 \times 10^{13} \text{ cm}^{-2}$ , is shown in Fig. 6. There are a couple of interesting points to note: 1) the effects of self-consistency, even at

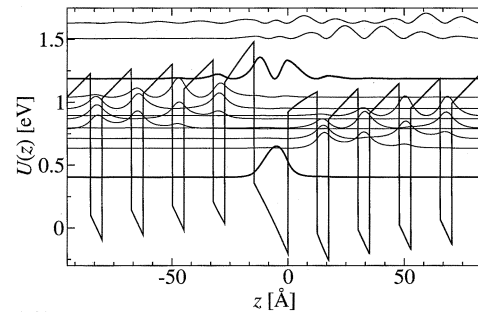


Fig. 6. Self-consistently calculated potential profile in a short BC structure (with four superlattice periods for confinement), having the same structural parameters as the optimal idealized structure (for  $\lambda \sim 1.55 \mu\text{m}$ ), but modulationally doped to  $1 \times 10^{13} \text{ cm}^{-2}$ . The wavefunctions of states present in this structure are also displayed.

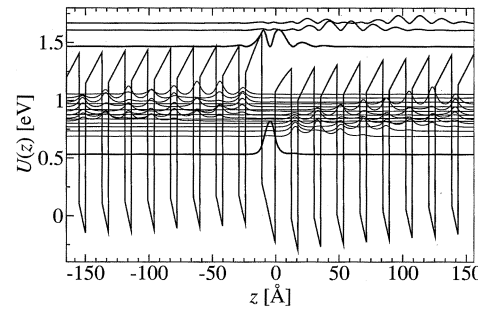


Fig. 7. Same as in Fig. 6, but for  $\lambda \sim 1.3 \mu\text{m}$ , with eight superlattice periods for confinement.

this high doping, are here rather mild, in contrast to the expectation that large electron density would introduce strong screening of the built-in field; this is because the built-in field is very large, and the wells are deep (wider wells, designed for longer wavelengths, would be much more affected); 2) the potential in the superlattice regions is not strictly periodic and, aside from the band bending due to self-consistency, there is a relatively small global slope present therein, which counterbalances the large potential drop across the central well, so to achieve periodic boundary conditions (this is due to finiteness of the structure, not to the self-consistency); 3) instead of lowest true miniband the finite structure has, on either side, a cluster of four states, localized in the four periods of the superlattice, and the same is true for higher minibands (a part of the next one is also shown in Fig. 6); the “minibands” on the two sides are mutually displaced in energy (have almost no overlap), but in spite of this and all the previous “imperfections” the two bound states remain strongly localized, with good overlap and hence the transition matrix element. One may therefore expect that the realistic structure is (close to) optimal, as was its idealized precursor. It is also important to note that this finite structure has all the electrons residing in the ground (localized) state, even at  $T = 300 \text{ K}$ , as is calculated from (27); this would not be the case for idealized infinite structure, where miniband population has to be considerable, as discussed in Section II. Similar conclusions apply to another example, the structure designed for absorption at  $\lambda \approx 1.3 \mu\text{m}$ , Fig. 7, again with modulation doping, which has 8 superlattice periods on each side to be able to confine the states with increased energies. If the doping of the central well only is employed, the positive charge of donor ions largely compensates

TABLE I

SUMMARY RESULTS OF SELF-CONSISTENTLY CALCULATED ABSORPTION PARAMETERS (ACTUAL PEAK ABSORPTION WAVELENGTH  $\lambda$  AND THE VALUE OF FRACTIONAL ABSORPTION  $A_{12}$ ) FOR REALISTIC FINITE BC STRUCTURES. THE DATA IN THE FIRST COLUMN DENOTE THE INITIALLY TARGETED  $\lambda$  AND THE DOPING TYPE (M—MODULATIONAL, W—CENTRAL WELL DOPING)

structure	$N_S$ [ $\text{cm}^{-2}$ ]	$\lambda$ [ $\mu\text{m}$ ]	$A_{12}$ [%]
1.55 $\mu\text{m}$ (M)	$2 \times 10^{12}$	1.519	0.166
1.55 $\mu\text{m}$ (M)	$1 \times 10^{13}$	1.583	0.964
1.55 $\mu\text{m}$ (W)	$2 \times 10^{12}$	1.492	0.128
1.55 $\mu\text{m}$ (W)	$1 \times 10^{13}$	1.476	0.575
1.30 $\mu\text{m}$ (M)	$2 \times 10^{12}$	1.296	0.237
1.30 $\mu\text{m}$ (M)	$1 \times 10^{13}$	1.327	1.080
1.30 $\mu\text{m}$ (W)	$2 \times 10^{12}$	1.283	0.233
1.30 $\mu\text{m}$ (W)	$1 \times 10^{13}$	1.269	1.110

that of electrons, and the band bending shown in Figs. 6 and 7 becomes even less prominent.

Finally, in Table I, the summary results of the self-consistently calculated characteristics of realistic, finite structures are given. The peak absorption wavelengths of finite BC structures are clearly quite close to the values initially targeted for the idealized infinite structure. The homogeneous linewidth was taken to be  $\Gamma = 60$  meV [8]. It is interesting to note that about half of the full linewidth originates from nonparabolicity effects, and the other half from homogeneous broadening.

#### IV. CONCLUSION

We have performed the design optimization of GaN–AlGaN Bragg-confined structures in order to maximize the intersubband absorption in the communications spectral range. An advantage offered by BC structures is the existence of bound states above the barrier top which is very important at shorter wavelengths. In particular, at  $\lambda \sim 1.3$   $\mu\text{m}$  the required content of Al in the barriers of the optimal structure is much lower than would be necessary for a simple quantum well. The effects of the built-in electrostatic field and band nonparabolicity were included in the first part (finding the optimal set of idealized, infinite BC structure parameters, using the simulated annealing algorithm), and the fully self-consistent calculation was performed subsequently for realistic, short-period structures, to check the quality of the design under heavy doping conditions.

#### ACKNOWLEDGMENT

The authors are grateful to the Royal Society (U.K.), and the Ministry of Science and Technology (Serbia) for support. Three of the authors, D. Indjin, Z. Ikonić, and P. Harrison, would also like to thank QEDI for advice on software implementation.

#### REFERENCES

- [1] S. Nakamura, M. Senoh, S. Nagahama, N. Iwasa, T. Yamada, T. Matsushita, Y. Sugimoto, and H. Kiyoku, “High-power, long-lifetime InGaN multi-quantum-well-structure laser diodes,” *Jpn. J. Appl. Phys.*, vol. 36, pp. L1059–L1061, 1997.
- [2] M. A. Khan, Q. Chen, M. S. Shur, B. T. McDermott, J. A. Higgins, J. Burm, W. J. Schaff, and L. F. Eastman, “CW operation of short-channel GaN/AlGaN doped channel heterostructure field effect transistors at 10 GHz and 15 GHz,” *IEEE Electron. Device Lett.*, vol. 17, pp. 584–585, 1996.
- [3] N. Iizuka, K. Kaneko, N. Suzuki, T. Asano, S. Noda, and O. Wada, “Ultrafast intersubband relaxation ( $\leq 150$  fs) in AlGaIn/GaN multiple quantum wells,” *Appl. Phys. Lett.*, vol. 77, pp. 648–650, 2000.
- [4] C. Gmachl, H. M. Ng, and A. Y. Cho, “Intersubband absorption in degenerately doped GaN/Al<sub>x</sub>Ga<sub>1-x</sub>N coupled quantum wells,” *Appl. Phys. Lett.*, vol. 79, pp. 1590–1592, 2001.
- [5] C. Gmachl, H. M. Ng, S. N. G. Chu, and A. Y. Cho, “Intersubband absorption at  $\lambda \sim 1.55$   $\mu\text{m}$  in well- and modulation-doped GaN/AlGaIn multiple quantum wells with superlattice barriers,” *Appl. Phys. Lett.*, vol. 77, pp. 3722–3724, 2000.
- [6] C. Gmachl, H. M. Ng, and A. Y. Cho, “Intersubband absorption in GaN/AlGaIn multiple quantum wells in wavelength range of  $\lambda \sim 1.75 - 4.2$   $\mu\text{m}$ ,” *Appl. Phys. Lett.*, vol. 77, pp. 334–336, 2000.
- [7] A. Ishida, T. Ose, H. Nagasawa, K. Ishino, Y. Inoue, and H. Fujiyasu, “Quantum cascade structure in AlN/GaN system assisted by piezoelectric effect,” *Jpn. J. Appl. Phys.*, vol. 41, pp. L236–L238, 2002.
- [8] K. Kishino, A. Kikuchi, H. Kanazawa, and T. Tachibana, “Intersubband transition in (GaN)<sub>m</sub>/(AlN)<sub>n</sub> superlattices in the wavelength range from 1.08 to 1.61  $\mu\text{m}$ ,” *Appl. Phys. Lett.*, vol. 81, pp. 1234–1236, 2002.
- [9] N. Suzuki and N. Iizuka, “Effect of polarization field on intersubband transition in AlGaIn/GaN quantum wells,” *Jpn. J. Appl. Phys.*, vol. 38, pp. L363–L365, 1999.
- [10] J. D. Heber, C. Gmachl, N. M. Ng, and A. Y. Cho, “Comparative study of ultrafast intersubband electron scattering times at  $\sim 1.55$   $\mu\text{m}$  wavelength in GaN/AlGaIn heterostructures,” *Appl. Phys. Lett.*, vol. 81, pp. 1237–1239, 2002.
- [11] J. L. Sanchez-Rojas, J. A. Garrido, and E. Muñoz, “Tailoring of internal fields in AlGaIn/GaN and InGaIn/GaN heterostructure devices,” *Phys. Rev. B*, vol. 61, pp. 2773–2778, 2000.
- [12] V. Fiorentini, F. Bernardini, F. Della Sala, A. Di Carlo, and P. Lugli, “Effects of macroscopic polarization in III–V nitride multiple quantum wells,” *Phys. Rev. B*, vol. 60, pp. 8849–8858, 1999.
- [13] S.-H. Park and S.-L. Chuang, “Spontaneous polarization effects in wurtzite GaN/AlGaIn quantum wells and comparison with experiment,” *Appl. Phys. Lett.*, vol. 76, pp. 1981–1983, 2000.
- [14] V. Jovanović, D. Indjin, Z. Ikonić, V. Milanović, and J. Radovanović, “Design of GaN/AlGaIn quantum wells for maximal intersubband absorption in  $1.3 < \lambda < 2$   $\mu\text{m}$  wavelength range,” *Solid State Commun.*, vol. 121, pp. 619–624, 2002.
- [15] V. D. Jovanović, Z. Ikonić, D. Indjin, P. Harrison, V. Milanović, and R. A. Soref, “Designing strain-balanced GaN/AlGaIn quantum well structures: application to intersubband devices at 1.3 and 1.55  $\mu\text{m}$  wavelengths,” *J. Appl. Phys.*, vol. 93, pp. 3194–3197, 2003.
- [16] V. Fiorentini, F. Bernardini, and O. Ambacher, “Evidence for nonlinear macroscopic polarization in III–V nitride alloy heterostructures,” *Appl. Phys. Lett.*, vol. 80, pp. 1204–1206, 2002.
- [17] E. Berkowicz, D. Gershoni, G. Bahir, E. Lakin, D. Shilo, E. Zolotayabko, A. C. Abare, S. P. Denbaars, and L. A. Coldren, “Measured and calculated radiative lifetime and optical absorption in In<sub>x</sub>Ga<sub>1-x</sub>N/GaN quantum structures,” *Phys. Rev. B*, vol. 61, pp. 10994–11008, 2000.
- [18] C. Sirtori, F. Capasso, J. Faist, and S. Scandolo, “Nonparabolicity and a sum rule associated with bound-to-bound and bound-to-continuum. Intersubband transitions in quantum wells,” *Phys. Rev. B*, vol. 50, pp. 8663–8674, 1994.
- [19] D. Indjin, V. Milanović, and Z. Ikonić, “Bragg-confined structures with conventional and effective-mass superlattices,” *Phys. Rev. B*, vol. 52, pp. 16762–16771, 1995.
- [20] J. Radovanović, D. Indjin, V. Milanović, and Z. Ikonić, “Resonant intersubband harmonic generation in asymmetric Bragg-confined quantum wells,” *Solid State Commun.*, vol. 110, pp. 339–343, 1999.
- [21] U. Ekenberg, “Nonparabolicity effects in quantum well: sublevel shift, parallel, and Landau levels,” *Phys. Rev. B*, vol. 40, pp. 7714–7726, 1989.
- [22] A. Corana, M. Marchesi, C. Martini, and S. Ridella, (1987) Minimizing multimodal functions of continuous variables with the “simulated annealing” algorithm. *ACM Trans. Math. Softw.*, pp. 262–280, [Online] Available: <http://www.netlib.org/opt/simann.f>

- [23] J. Radovanović, V. Milanović, Z. Ikonić, and D. Indjin, "Quantum-well profile optimization for maximal Stark effect and application to tunable infrared photodetectors," *J. Appl. Phys.*, vol. 91, pp. 525–527, 2002.
- [24] S. N. Mohammad, A. A. Salvador, and H. Morkoc, "Emerging gallium nitride based devices," *Proc. IEEE*, vol. 83, pp. 1306–1355, 1995.
- [25] G. Martin, A. Botchkarev, A. Rockett, and H. Morkoc, "Valence-band discontinuity of wurtzite GaN, AlN, and InN heterojunctions measured by x-ray photoemission spectroscopy," *Appl. Phys. Lett.*, vol. 68, pp. 2541–2543, 1996.
- [26] S.-H. Wei and A. Zunger, "Valence band splitting and band offsets of AlN, GaN, and InN," *Appl. Phys. Lett.*, vol. 69, pp. 2719–2721, 1996.
- [27] F. Bernardini and V. Fiorentini, "Nonlinear macroscopic polarization in III–V nitride alloys," *Phys. Rev. B*, vol. 64, pp. 1–7, 2001.

**Jelena Radovanović** was born in Belgrade, Yugoslavia, in 1973. She received the B.Sc., M.Sc., and Ph.D. E.E. degrees from the Faculty of Electrical Engineering, University of Belgrade, Belgrade, Yugoslavia, in 1997, 1999, and 2001, respectively.

She is an Assistant Professor with the Faculty of Electrical Engineering, University of Belgrade, and an Assistant Research Professor at the Institute of Physics, University of Belgrade. Her research interests include the optimization of nonlinear optical properties of semiconductor quantum wells and Bragg-confined structures.

**Vitomir Milanović** was born in Svetozarevo, Yugoslavia, in 1947. He received the B.Sc, M.Sc, and Ph.D. degrees in electrical engineering from the University of Belgrade, Belgrade, Yugoslavia, in 1971, 1977, and 1983, respectively.

He is currently a Full Professor with the Faculty of Electrical Engineering, University of Belgrade. His research interests include the electronic structure and optical properties of quantum wells and superlattices.

**Zoran Ikonić** was born in Belgrade, Yugoslavia, in 1956. He received the B.Sc., M.Sc., and Ph.D. degrees in electrical engineering from the University of Belgrade, Belgrade, Yugoslavia, in 1980, 1984, and 1987, respectively.

Since 1981, he has been with the Faculty of Electrical Engineering, University of Belgrade, where since 1998 he has been a Full Professor. In 1999, he joined the Institute of Microwaves and Photonics, University of Leeds, Leeds, U.K. His research interests include the electronic structure, optical and transport properties of semiconductor nanostructures, and devices based upon them.

**Dragan Indjin** was born in Zemun, Yugoslavia, in 1963. He received the B.Sc., M.Sc., and Ph.D. degrees in electrical engineering from the University of Belgrade, Belgrade, Yugoslavia, in 1988, 1993, and 1996, respectively.

He currently holds the position of Associate Professor at the Faculty of Electrical Engineering, University of Belgrade. In 2001, he joined the Institute of Microwaves and Photonics, University of Leeds, Leeds, U.K. His research interests include the electronic structure, optical, and transport properties of quantum wells, superlattices, and quantum cascade structures from near- to far-infrared spectral range.

**Vladimir Jovanović** was born in Belgrade, Yugoslavia, in 1978. He received the B.Sc. degree in electrical engineering from the University of Belgrade, Belgrade, Serbia and Montenegro, in 2002. He is currently working toward the Ph.D. degree at the Institute of Microwaves and Photonics, School of Electronic and Electrical Engineering, University of Leeds, Leeds, U.K., in the field of GaN-based near-infrared and terahertz intersubband devices.

**Paul Harrison (SM'99)** received the B.Sc. degree from the University of Hull, Hull, U.K., in 1988, and the Ph.D. degree from the University of Newcastle-upon-Tyne, U.K., in 1991.

He was a Postdoctoral Research Assistant at the University of Hull until 1995, when he obtained a Fellowship at the University of Leeds, Leeds, U.K. Since joining the Institute of Microwave and Photonics, University of Leeds, he has been researching ways to adapt his theoretical and computational experience in semiconductor heterostructures to terahertz sources and detectors. He currently holds a Chair in Quantum Electronics. He is the author of the book *Quantum Wells, Wires and Dots* (Chichester, U.K.: Wiley, 1999).